JOURNAL OF GUIDANCE, CONTROL, AND DYNAMICS
Vol. 34, No. 3, May–June 2011

Analysis of Flexible Aircraft Dynamics Using Bifurcation Methods

N. Baghdadi,* M. H. Lowenberg,† and A. T. Isikveren‡
University of Bristol, Bristol, England BS8 1TR, United Kingdom

DOI: 10.2514/1.51468

Modern commercial aircraft designs are continuously driven towards more slender wing configurations in order to meet performance and general mission requirements. Consequently, these aircraft are characterized by flexible structures that undergo large deformations, and in turn the frequency separation between the flexible and rigid-body modes is greatly reduced. The associated coupling can, in the presence of nonlinearities, introduce effects on the flight dynamics of such vehicles that conventional methods may not adequately predict, leading to the potential of degraded handling qualities. This paper evaluates the effects of flexibility on the dynamics, stability, and control of elastic aircraft using an analysis framework based on bifurcation and continuation tools, linked to classical analysis methods. Results based on variations of a Rockwell B1 model demonstrate the suitability of the approach in revealing dynamic coupling between rigid-body and flexible modes in regions of the flight envelope in which nonlinearities are significant. Furthermore, the efficiency of this approach relative to traditional nonlinear simulation is discussed. The robustness of idealized control law designs to unmodeled elastic modes is also investigated.

Nomenclature

b	=	wing span, m
C_{M_0}, C_{Z_0}	=	pitching moment and normal force coefficients
$C_{M(.)}$, $C_{X(.)}$, $C_{Z(.)}$	=	pitching moment, axial and normal force derivatives due to (.)
$C^{\eta_i}_{(.)}$	=	generalized aerodynamic derivative due to (.) associated with the ith elastic mode
c	=	mean aerodynamic chord, m
I_{yy}	=	body axes moments of inertia, kg · m^2
K	=	gain matrix
M	=	aircraft mass, kg
M_T	=	moment due to thrust, kg
m_i	=	modal mass associated with the ith elastic mode, kg · m^2
p, q, r	=	body axis roll, pitch, and yaw rates, rad/s
Q_L, Q_M, Q_N	=	total rolling, pitching and yawing moments, Nm
Q_X, Q_Y, Q_Z	=	total aerodynamic force along the x, y and z body axes, N
Q_{η_i}	=	generalized force associated with coordinate i, N
S	=	wing reference area, m^2
T	=	thrust, N
U, V, W	=	component of total velocity along the x, y, and z body axes, m/s
$\boldsymbol{u}$	=	general control vector
V_T	=	total velocity, m/s
x_e, y_e, z_e	=	aircraft center of gravity earth axes coordinate positions, m
$\boldsymbol{x}$	=	general state vector
α	=	angle of attack, deg
α_{com}	=	commanded angle of attack, deg
β	=	angle of sideslip, deg
δ_{cv}	=	control vane deflection angle, deg
δ_{SHT}	=	symmetric horizontal tailplane deflection angle, deg
ζ	=	damping ratio
η	=	generalized displacement
Λ	=	leading-edge sweep angle, deg
λ	=	system eigenvalues
ρ	=	air density, kg/m^3
ϕ, θ, ψ	=	Euler bank, pitch, and heading angles, deg
ω	=	natural frequency, rad/s

Superscripts

.	=	d( )/dt
..	=	d^2( )/dt

Presented as Paper 2010-2950 at the 51st AIAA/ASME/ASCE/AHS/ASC Structures, Structural Dynamics, and Materials Conference, Orlando, FL, 12–15 April 2010; received 7 July 2010; revision received 22 October 2010; accepted for publication 16 November 2010.

*Ph.D. Student, Department of Aerospace Engineering. Student Member AIAA.

†Senior Lecturer, Department of Aerospace Engineering. Senior Member AIAA.

‡Senior Lecturer, Department of Aerospace Engineering; currently Head, Radical Aircraft Concepts, Bauhaus Luftfahrt, D-80807 München, Germany. Senior Member AIAA.

I. Introduction

NONLINEAR problems in aircraft flight dynamics have been well recognized and widely documented. The traditional analysis approach assumes a sufficiently large margin that separates the natural frequencies of the rigid-body modes of the aircraft and its lowest elastic modes. This is generally an acceptable assumption that allows the use of rigid-body models for aircraft exhibiting a sufficient level of rigidity, and typically the lowest structural natural frequencies of such aircraft are in the region of 5.0 Hz [1]. Modern commercial aircraft designs are continuously driven towards more slender wing configurations in order to meet performance and mission requirements. Consequently, these aircraft are characterized by flexible structures that undergo large deformation induced displacements and accelerations, and in turn, the frequency separation between the flexible and rigid-body modes is greatly reduced. In such cases, a strong coupling between the rigid-body and structural dynamics of the aircraft may occur affecting the overall stability and handling qualities. In many instances, in particular where there are nonlinearities in the system, the conventional approach may no longer be sufficient. For example, the aerodynamics may be nonlinear in novel aircraft configurations, and the extended use of gust and manoeuvre load alleviation systems (to reduce wing weight), can exacerbate the influence of structural nonlinearity. This means a more advanced analysis technique may be required to accurately capture the effects of flexible modes on the flight dynamics of such vehicles to allow a better understanding of the induced nonlinear behavior in order to ease control system designs. Since the 1970s, numerous research efforts investigated different approaches to couple elasticity and flight mechanics problems. Typically, the focus

was on augmenting linear structural modeling with the rigid-body dynamics.

Meriovich and Tuzcu [2] presented a unified theory to model flexible aircraft dynamics based on fundamental principles and incorporating both the rigid-body motions and the elastic deformations, and the couplings thereof, as well as the aerodynamic, propulsion, control and gravity forces. The formulation is hybrid in nature, and consists of ordinary differential equations for the rigid-body translations and rotations of the aircraft and partial differential equations to represent the elastic deformations of the flexible components, such as the fuselage, wing and empennage. Such a modeling approach allows the problem to be subdivided into a nonlinear flight dynamics problem for rigid-body motions and a structural dynamics problem in order to estimate the elastic deformations and perturbations of the rigid-body translations and rotations. Solutions of the first problem are then fed into the second problem. The authors in [2] demonstrate the use of their formulation on a practical example.

Waszak and Schmidt [3] developed the nonlinear equations of motion for an elastic aircraft from first principles using Lagrange's equation and the principle of virtual work. A mean axes reference system was used which allows the linear and angular momentum vectors due to elastic deformation to vanish, and all the coupling between the rigid-body and elastic degrees of freedom is achieved by means of the aerodynamic loading. The authors used a linearized aerodynamic strip method to derive a quasi-steady closed-form expression of the generalized aerodynamic forces and moments. A parametric study of the flexibility effects was applied to a generic example of an elastic aircraft.

In [4], Schmidt and Raney extended this work and demonstrated the importance of coupled flight dynamics and structural dynamics by showing the resulting impacts on handling qualities using Cooper–Harper pilot ratings for a simulated Rockwell B1 aircraft as a result of coupling rigid-body dynamics and flexible structures. Experimental results obtained from motion-based piloted simulations of the vehicle clearly revealed the potential for a dangerous form of dynamic interaction referred to as "biodynamic coupling." In essence, the combination of the aeroelastic aircraft, the control stick, and the pilot's biomechanical dynamics may result in a closed-loop system that is unstable or lightly damped. In such instances, cockpit vibrations may cause resonance of the pilot's biodynamic frame, resulting in sustained feedthrough of aeroelastic vibrations back into the control stick. Etkin and Reid [5] and Wright and Cooper [1] both presented a similar modeling approach using the method of normal modes. The mean axes reference system was adopted and the traditional rigid-body equations of motion were altered through additional aerodynamic terms resulting from aeroelasticity.

In all these aircraft models various nonlinearities are involved, such as those due to rigid-body motions and aerodynamic forces. Although most of these studies successfully implemented simulation models capable of analyzing the effects of flexibility on the overall dynamics, the scope was usually limited since the stability characteristics were determined for individual flight conditions. No attempt has been made to determine the underlying dynamics of these effects and their parameter dependence through regions of the flight envelope where the inherent nonlinear behavior of an aircraft model is significant. The use of a more powerful tool becomes an important contribution towards achieving a qualitative understanding of the stability, control and handling qualities of flexible aircraft.

Since the early 1980s, considerable progress in the application of bifurcation theory and numerical continuation methods as a means of analyzing nonlinear aircraft behavior has been observed. Development of advanced computational software [6,7] facilitates the successful application of these methods and permits a better understanding of the nonlinear dynamic problems at hand. For smooth continuous dynamic systems, continuation methods form the basis of numerical tools for implementation of bifurcation theory. Carroll and Mehra [8] were the first to link observed nonlinear phenomena to mathematical bifurcations. Several subsequent contributions [9–16] demonstrated efficient applications of the methods to both open-loop and closed-loop aircraft dynamics problems. A review of the recent results in the application of bifurcation and continuation methods to flight dynamics problems is given in [17]. Besides its use in analyzing aircraft flight dynamics, the bifurcation and continuation method has also been successfully employed in studying the behavior of aeroelastic systems, in particular, the existence of limit cycle oscillations (LCOs) in wings having structural and aerodynamic nonlinearities [18–20].

Siepenkötter and Alles [21] investigated the nonlinear characteristics of a model with the interaction of flight dynamics and structural modes, but only considered equilibria. In this paper, we present a more comprehensive framework for the analysis of flexible aircraft dynamics based on the use of bifurcation and continuation tools linked to classical analysis methods. In the presence of nonlinearities, the efficiency of this framework in revealing changes in the qualitative dynamics of flexible vehicles will be demonstrated. The modeling approach used in [3] is adopted. The full-nonlinear equations of motion governing elastic aircraft dynamics developed using Lagrange's equation and the principle of virtual work are implemented and tested using MATLAB/Simulink software. The parametric analysis presented in [3] yielding three versions of an elastic vehicle (based on the Rockwell B1 aircraft) with varying levels of flexibility is used. Using these B1 models, numerical continuation is applied in order to investigate the resulting effects on the global stability of the aircraft. Unaugmented aircraft bifurcation diagrams are presented for longitudinal flight at various flight conditions. These indicate the need for stability augmentation for which idealized control laws are designed; eigenstructure assignment (EA) is used to attempt to decouple the rigid-body and elastic modes. Under normal conditions, these control laws effectively linearize the system and provide desired characteristics. We show that where the actual system differs from that for which the control laws were defined, via different structural mode definitions, nonlinear behavior is reintroduced. The bifurcation analysis is then demonstrated to be efficient in identifying the nonlinearities and explaining the resulting behavior.

II. Aircraft Model

The study vehicle is similar to an early version of the Rockwell B1 high-speed bomber, which is regarded to be representative, in terms of dynamic characteristics, to advanced transport aircraft concepts [22]. The aircraft was considered in the current study for its degree of structural flexibility and the availability of structural dynamic analysis results, i.e., vibration frequencies and mode shapes. Furthermore, a nonlinear simulation model that was used in a NASA study is available in [22,23].

The aircraft equations of motion are defined using the methodology developed by Waszak and Schmidt [3] for flexible aircraft. The complete set of dynamic equations that describe the flexible aircraft motion include the 12 nonlinear first-order differential equations for the dynamics of a rigid-body in six degrees of freedom, plus a set of second-order differential equations describing the structural modes. The state vector in this case is $\boldsymbol{x} = [\alpha, \beta, V_T, p, q, r, \phi, \theta, \psi, x_e, y_e, z_e, \eta_i]$, where the axes sign conventions for the rates and velocities are shown in Fig. 1; other states follow standard conventions. In this paper only longitudinal dynamics of the aircraft are considered, and since it is the faster flight mechanics modes that are likely to couple with the flexible modes, the aircraft rigid-body dynamics is represented in a second-order form (capturing the short period mode).

The structural flexibility of the Rockwell B1 model is defined in terms of free vibration modes of the structure (often referred to as normal modes). Four symmetric modes are incorporated in the model with the corresponding modal masses and damping ratios for each mode listed in Table 1. The generalized displacement coordinates, η_i, $i = 1, 2, 3, 4$, for each mode are referenced relative to the most forward mass point of the fuselage reference line labeled as datum in Fig. 1.

Figure 2 defines the sign conventions used in association with the normal modes and the locations of the structural points on the aircraft

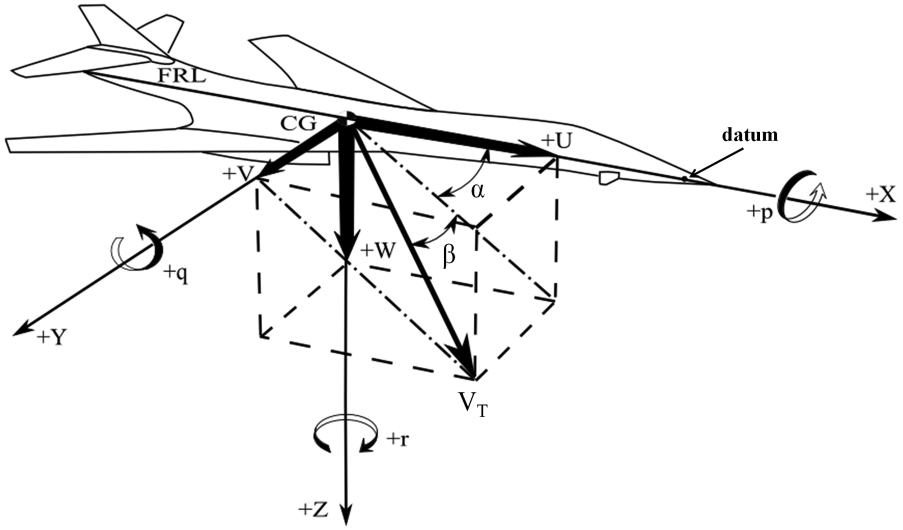

Fig. 1 Sign convention for rates and velocities in body axes, adapted from [25].

at which the elastic displacements are computed. The reduced system is represented by

$$\dot{q} = \frac{Q_M}{I_{yy}} \tag{1}$$

$$\dot{\alpha} = q + \frac{Qz}{MV_T \cos\beta} \tag{2}$$

$$\ddot{\eta}_i + 2\zeta_i \omega_i \dot{\eta}_i + \omega_i^2 \eta_i = \frac{Q\eta_i}{m_i} \tag{3}$$

The coupling between the rigid-body and the flexible modes occurs via the aerodynamic forces and moments which are expressed as

$$Q_Z = \frac{\rho V_T^2 S}{2}(C_{Z_0} + C_{Z_\alpha}\alpha + C_{Z_{\delta_{\mathrm{SHT}}}}\delta_{\mathrm{SHT}} + C_{Z_{\delta_{\mathrm{cv}}}}\delta_{\mathrm{cv}} + \Sigma_{i=1}^{4} C_{Z_{\eta_i}}\eta_i) + \frac{\rho V_T S c}{4}(C_{Z_q} q + \Sigma_{i=1}^{4} C_{Z_{\dot{\eta}_i}}\dot{\eta}_i) \tag{4}$$

$$Q_M = \frac{\rho V_T^2 S c}{2}(C_{M_0} + C_{M_\alpha}\alpha + C_{M_{\delta_{\mathrm{SHT}}}}\delta_{\mathrm{SHT}} + C_{M_{\delta_{\mathrm{cv}}}}\delta_{\mathrm{cv}} + \Sigma_{i=1}^{4} C_{M_{\eta_i}}\eta_i) + \frac{\rho V_T S c^2}{4}(C_{M_q} q + \Sigma_{i=1}^{4} C_{M_{\dot{\eta}_i}}\dot{\eta}_i) + M_T \tag{5}$$

Table 1 Geometry, mass, inertia, and vibration mode data of the study vehicle [3]

Parameter	Value
Flight condition	
Mach	0.6
Altitude	5000 ft (1254 m)
V_T	200 m/s (390 KTAS)
Vehicle geometry and mass properties	
c	4.66 m
S	181 m^2
M	131×10^3 kg
b	21.3 m
Λ	65 deg
I_{yy}	8.68×10^6 kg $\cdot$ m^2
Modal generalized masses	
m_1	249 kg $\cdot$ m^2
m_2	13.0×10^3 kg $\cdot$ m^2
m_3	1.81×10^3 kg $\cdot$ m^2
m_4	5.91×10^3 kg $\cdot$ m^2
Modal damping ratios	$\zeta_i = 0.02$, $i = 1, 2, 3, 4$

$$Q = \frac{\rho V_T^2 S c}{2}(C_0^{\eta_i} + C_\alpha^{\eta_i}\alpha + C_{\delta_{\mathrm{SHT}}}^{\eta_i}\delta_{\mathrm{SHT}} + C_{\delta_{\mathrm{cv}}}^{\eta_i}\delta_{\mathrm{cv}} + \Sigma_{j=1}^{4} C_{\eta_j}^{\eta_i}\eta_j) + \frac{\rho V_T S c^2}{4}(C_q^{\eta_i} q + C_{\dot{\alpha}}^{\eta_i}\dot{\alpha} + \Sigma_{j=1}^{4} C_{\dot{\eta}_j}^{\eta_i}\dot{\eta}_j) \tag{6}$$

Note that these forces and moments are nonlinear functions of angle of attack, α over the range for which the aerodynamic model is defined, namely $-10^\circ \le \alpha \le 20^\circ$ (see examples in Fig. 3, chosen to exemplify the nature of the nonlinearities). The generalized forces are, however, constant for the full range of α, as per [23].

The simulation model is implemented using MATLAB/Simulink software and consists of the equations of motion, tabulated nonlinear aerodynamic coefficients, stability and control augmentation system (SCAS), and a nonlinear engine model [22,23]. To comply with the requirement that the model is smooth for bifurcation and continuation analysis, cubic splines are fitted to the tabulated data, and used to generate aerodynamic loads (including the plots in Fig. 3). The aircraft has several control effectors. In this work, only the longitudinal control effectors were considered, namely, the symmetric horizontal tail deflection δ_{SHT} (deg), thrust T (N) via power lever angle (PLA), and control vanes δ_{cv} (deg), available below the pilot station to improve ride quality. Sign convention for the aerodynamic forces, moments and control effector deflection angles are shown in Fig. 4.

Waszack and Schmidt [3] considered different versions of the Rockwell B1 model with varying levels of flexibility, by parametrically reducing the in vacuo (isolated) frequencies of vibration of the structural modes. Here, these configurations are analyzed, representing a hypothetical family of the Rockwell B1 aircraft that differ only in the amount of structural rigidity; they can be regarded physically as vehicles with identical external geometries but with different internal structural geometry and/or materials such that the vibration frequencies are changed while the mode shapes remain the same (see Table 2).

Configuration C1 is the model of the baseline flexible aircraft, and C2 was obtained by lowering the frequencies of vibration of C1. C0 represents the rigid model and is obtained by ignoring the flexible modes in the model, i.e., only rigid-body states are included.

Table 2 Study vehicle configurations [3]

Configuration	Symmetric 1 ω_1, rad/s	Symmetric 2 ω_2, rad/s	Symmetric 3 ω_3, rad/s	Symmetric 4 ω_4, rad/s
C0 (rigid)	——	——	——	——
C1 (baseline)	12.6	14.1	21.2	22.0
C2 (modified)	6.29	7.04	10.6	11.0

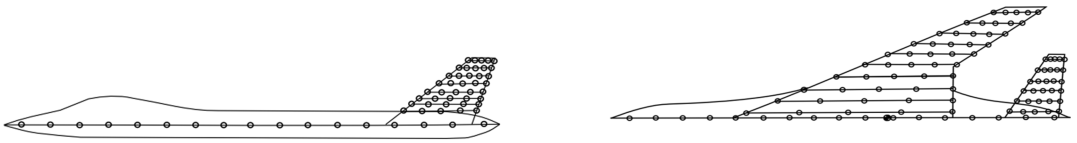

a) Structural mass control points. Adapted from Ref. 24

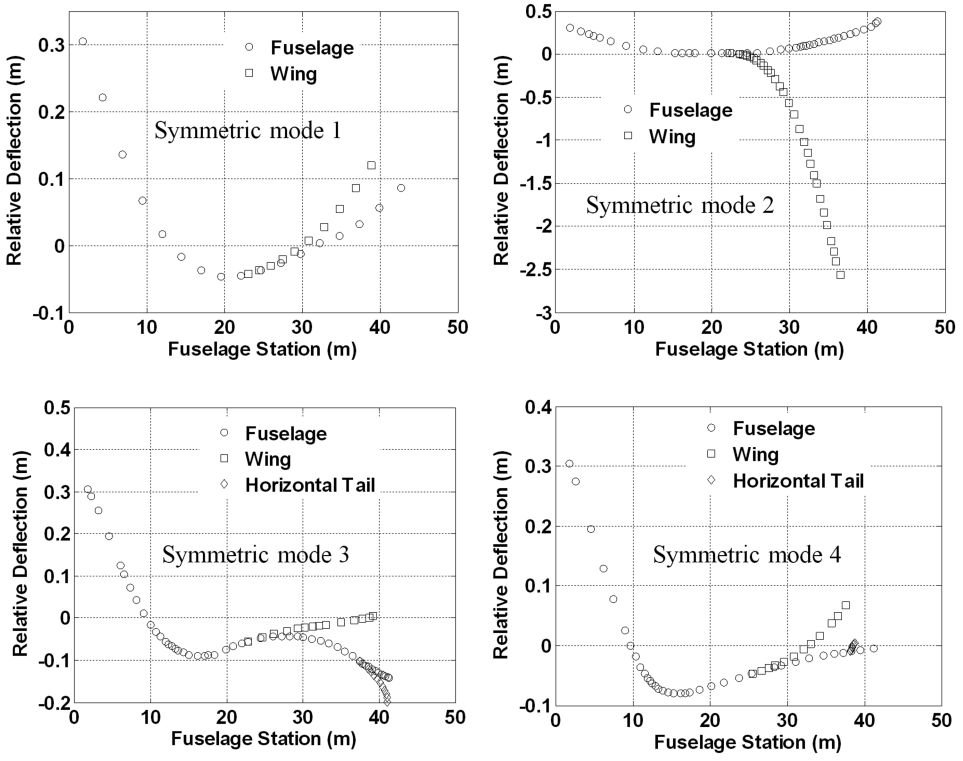

b) Example of symmetric mode shapes for $\eta_i = 1$, (i=1,..,4),V_T=200 m/s (390 KTAS, Mach = 0.60)

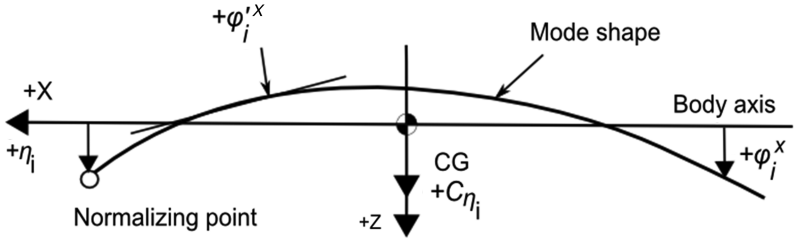

c) Structural mode deflections, slopes and generalized force sign convention. Adapted from Ref. 24

Fig. 2 Aircraft geometric and structural data [3,23,25].

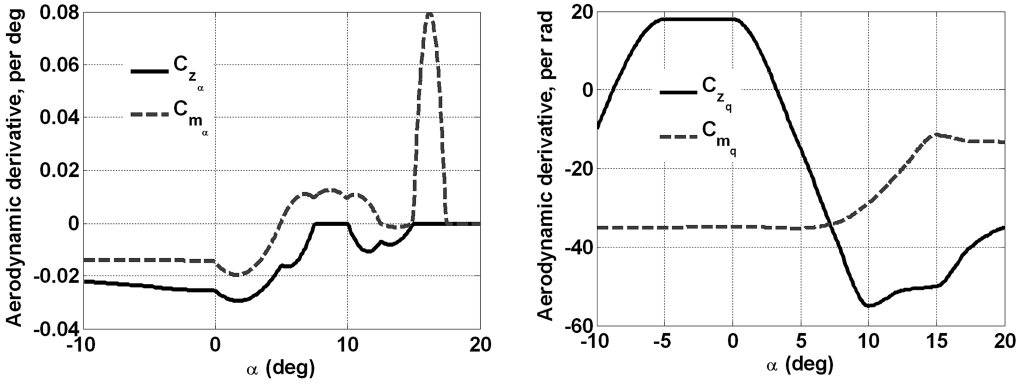

a) Aerodynamic derivatives due to angle of attack b) Aerodynamic derivatives due to pitch rate

Fig. 3 Sample aerodynamic derivatives plotted for the defined angle of attack range.

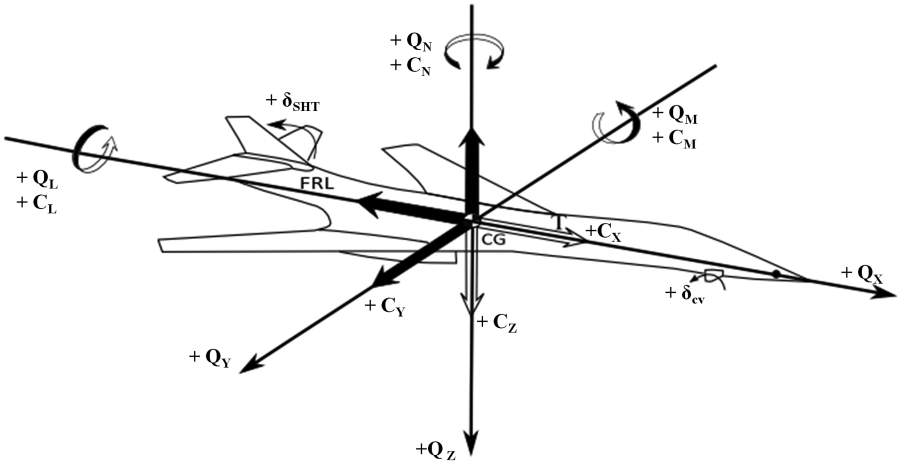

Fig. 4 Sign convention for aerodynamic forces, moments and control surface deflections, adapted from [25].

Note that the simulation models implemented for C1 and C2 configurations incorporate the same equations of motion, namely Eqs. (1–6), and only the frequencies of symmetric flexible modes differ between the two models, as defined in Table 2. The simulation model for C0 incorporates Eqs. (1), (2), (4), and (5) (i.e., elastic degrees of freedom are set to zero).

III. Bifurcation and Continuation Analysis

In this section, a brief description of the bifurcation and continuation methods is provided along with details of the implementations used in this work.

A. Bifurcation Methods

Bifurcation analysis represents one of the key methodologies of dynamic system theory for studying systems of smooth nonlinear ordinary differential equations. It provides a global picture of the steady states of such a dynamic system, and their stability over a range of parameter/input conditions. The flexible aircraft model described in the previous section can be written as a set of n autonomous ordinary differential equations:

$$\dot{\boldsymbol{x}} = \boldsymbol{f}(\boldsymbol{x}, \boldsymbol{u}) \qquad \boldsymbol{f}, \boldsymbol{x} \in \Re^n \qquad \boldsymbol{u} \in \Re^m \tag{7}$$

where n corresponds to the number of components of the state vector, $\boldsymbol{x}$, and represents the dimension of the system; m is the number of components of the input (control) parameter vector of the system, $\boldsymbol{u}$. The variable, $\dot{\boldsymbol{x}}$ is the state derivative vector and $\boldsymbol{f}$ is a set of nonlinear continuous functions. Implementation of the bifurcation analysis involves generating steady-state solutions in state parameter space. Local stability information is also generated, and bifurcation theory enables this to be interpreted in terms of the global behavior of the system. A bifurcation is said to occur when the system exhibits a change in local stability and its influence can be either local or global in nature. Such information on steady states of a nonlinear aircraft model aids the understanding of its behavior by revealing the underlying dynamics of the system. Here, one first considers fixed points (or equilibria) steady states in which case Eq. (7) is solved for

$$\boldsymbol{f}(\hat{\boldsymbol{x}}, \boldsymbol{u}) = 0 \tag{8}$$

in order to obtain an equilibrium state vector, $\hat{\boldsymbol{x}}$, corresponding to the parameters, $\boldsymbol{u}$. In addition, periodic orbits, which are another example of nonlinear steady-state behavior, are computed. The onset of a periodic solution is usually a Hopf bifurcation from an asymptotically stable system. The Hopf bifurcation is characterized by a complex conjugate pair crossing the imaginary axis. It can either be "supercritical," in which case the trajectory will diverge (locally) from the unstable equilibria onto the stable LCO borne at the Hopf point, or it can also be "subcritical," resulting in an unstable LCO; i.e., trajectories that begin inside the LCO decay onto the equilibrium solution stable branch, whereas, trajectories outside the unstable LCO grow until they interact with other attractors. Stability of periodic orbits can be calculated via the use of characteristic (Floquet) multipliers. If linear stability analysis is performed, it will show that locally the system is unstable. A periodic orbit is characterized by $\dot{\boldsymbol{x}}(t) = \dot{\boldsymbol{x}}(t + T)$, where, T, is the period of the orbit. If a local cross section is taken transversally to the flow, one dimension lower than that of the phase space, then the map of intersections with the flow is called a Poincaré section. The map itself can be defined as $\boldsymbol{x}_{i+1} = \boldsymbol{F}(\boldsymbol{x}_i)$. The behavior of the local flow is determined by the eigenvalues of the Jacobian matrix, $\boldsymbol{F}$, and these eigenvalues are called the characteristic multipliers. A periodic orbit is said to be stable if the moduli of all multipliers are less than unity, otherwise, if the modulus of at least one multiplier is larger than unity, it is unstable. Specific details of the eigenvalues crossing the imaginary axis, or multipliers crossing the unit circle, dictate the type of bifurcation that arises. An important characteristic of nonlinear dynamic systems is the presence of multiple steady-state solutions for a given parameter (input) set. The reader is referred to texts such as Strogatz [24] for a comprehensive introduction to bifurcation theory.

B. Numerical Continuation Method

Implementation of bifurcation analysis is achieved via continuation methods. These are path following algorithms which, given a starting solution, can trace out a curve of steady states as a parameter varies, e.g., a control surface deflection. An initial solution must be supplied to the algorithm such that it can then generate bifurcation diagrams by solving for paths of steady-state solutions as the parameter varies, and simultaneously monitors the stability of the system. Different approaches can be used to locate the starting solutions. For instance, one could perform a time history simulation with the continuation parameter (CP), held constant until the system settles to an equilibrium or a stable LCO, or use a minimization routine to trim the system. Software packages such as AUTO [6] used in this work facilitate the application of bifurcation methods using the numerical continuation technique. One-parameter bifurcation diagrams are generated to show the variation of fixed points of a dynamic system and their stability as the CP is varied: each state variable is usually plotted separately against the CP, i.e., as two-dimensional projections of the state parameter space. The local stability of the fixed points is indicated by line type, and for the periodic orbits by solid or empty circles as shown in Fig. 5 which defines the convention used throughout this paper unless otherwise indicated. Note that secondary branches of periodic solutions emanate from the period doubling bifurcations in Fig. 5; however, these are not shown. Briefly, the bifurcation points (BPs) shown in this plot may be described as follows:

1) Fold: two equilibria solutions exist for the same value of the CP, and these coalesce as the CP approaches the fold point. If the CP

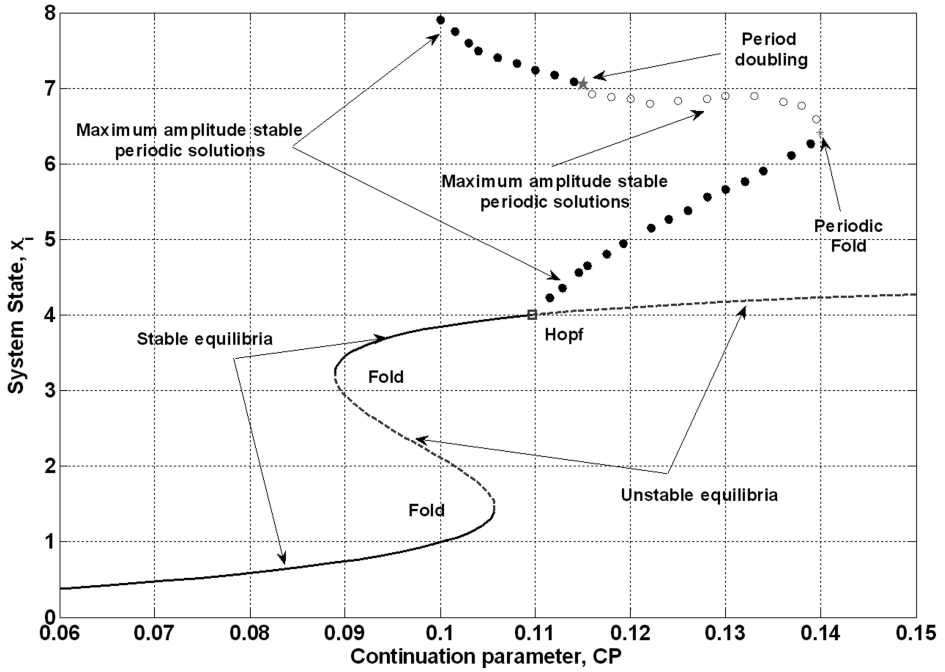

Fig. 5 Sample bifurcation diagram showing different bifurcations and stability types generated using a continuation algorithm for equilibria and periodic solutions (maximum amplitude of orbit).

moves beyond the fold, which occurs when a real root crosses the imaginary axis, then there no longer exist any local equilibria and the system will typically undergo a jump phenomenon to a different region of state space.

2) Hopf: this occurs when a conjugate pair of eigenvalues crosses the imaginary axis and is the onset point for periodic solutions (limit cycles).

3) Periodic fold: two periodic orbits exist (one stable and the other unstable), which coalesce at the BP. It is analogous to the fold bifurcation of equilibria.

4) Period doubling: this is the onset of a new branch of periodic orbits with twice the period of the original orbit.

IV. Unaugmented Aircraft Analysis

In the results shown in this section, the controller is not used and the CP is δ_{SHT}. Note that the only steady-state solution branches shown here are those on the symmetric flight trim branch, i.e., no spin/autorotation branches, and these are solved over the full range of α for which the aerodynamics in the model is defined, i.e., $\alpha = -10$ to 20°.

A. Rigid-Body Analysis

Figure 6 shows the bifurcation diagrams of the second-order rigid-body model. The results show quite unusual behavior, with unstable solutions over much of the α range and a number of bifurcations which are summarized in Table 3. These bifurcations are directly linked to changes in longitudinal stability, i.e., C_{m_α} (see Fig. 3a). Note also that q would be zero throughout the CP range in a higher-order model that includes the Phugoid dynamics (where the body angular velocity $\dot{\theta} = 0$ equation is included) but not in the short period approximation used here.

Starting from the lower saturation point of the equilibria at $\alpha = -10.0°$, and working up the trim branch, the system is stable until it reaches a fold at $\alpha = 5.19°$. This fold is associated with a change in static pitch stability and the system remains unstable until it reaches another fold bifurcation at $\alpha = 12.3°$. The aircraft regains stability but only for a small range of values since the system folds once again at $\alpha = 15.1°$. The stability of the system is lost and it remains so until the upper saturation point at $\alpha = 20°$ is reached.

Table 3 Unaugmented rigid-body model BPs

Label	Type	CP δ_{SHT}, deg	α, deg	q, deg/s
1	Fold	−8.75	5.19	1.89
2	Fold	−6.12	12.3	3.25
3	Fold	−6.75	15.1	3.52

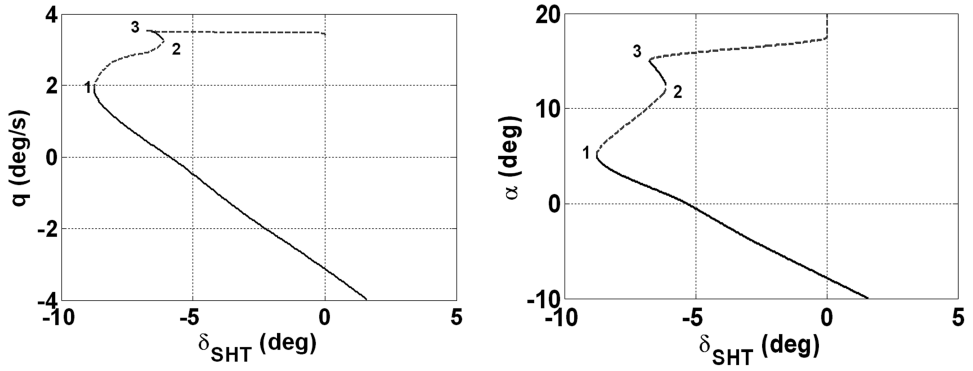

a) Pitch rate **b) Angle of attack**

Fig. 6 Bifurcation diagrams of the unaugmented, rigid-body model. BPs are labeled 1–3 and detailed in Table 3.

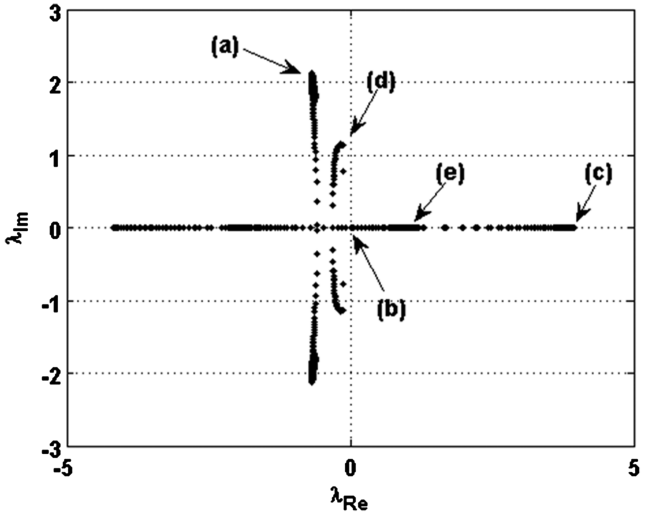

Fig. 7 Movement of the unaugmented, rigid-body model short period mode roots for the defined CP range.

Figure 7 shows the movement of the short period mode eigenvalues along the solutions shown in Fig. 6, from low to high α. At negative and low positive α, namely, $-10.0^\circ \leq \alpha \leq 4.98^\circ$, the short period mode is a complex pair, point (a), and as the CP is varied the frequency decreases until the conjugate pair meet on the real axis and split into two real roots. One root moves into the right-half plane, point (b), giving rise to a fold bifurcation, i.e., label 1 in Table 3. It continues to move right until it reaches a maximum, point (c), it then reverses direction and crosses the imaginary axis again causing the second fold (BP label 2 in Table 4). The short period mode then becomes, once again, oscillatory, point (d), but only for a short range of α, values, namely, $12.4^\circ \leq \alpha \leq 15.1^\circ$, as the stability is lost through fold bifurcation 3 when the short period mode dissociates into two real roots. One root crosses the imaginary axis and moves to the right-half plane where it remains until the CP saturates (e) when α reaches its upper limit of 20°. It is highlighted that without the SCAS, the aircraft model is not stable above $\alpha \approx 5^\circ$, except for a small range between $\alpha = 12.5$ and 15°. Furthermore, the handling qualities are clearly poor over much of the α range.

Table 4 Cooper–Harper level 1 handling qualities design targets for the SCAS-C1

Aircraft mode	Eigenvalue λ_i	Undamped natural frequency ω_i, rad/s	Damping ratio ζ_i
Short period	$-1.50 \pm 1.50i$	2.12	0.70
Flexible mode 1	$-0.52 \pm 12.4i$	12.4	0.04
Flexible mode 2	$-2.67 \pm 17.8i$	17.9	0.14
Flexible mode 3	$-0.44 \pm 21.2i$	21.2	0.02
Flexible mode 4	$-0.30 \pm 22.0i$	22.0	0.01

B. Flexible Body Analysis

To demonstrate the effects of flexibility on the dynamics of the aircraft, selected bifurcation diagrams of the second-order system for the C1 configuration were generated. The same bifurcations seen in the rigid case occur but at slightly different values of α, as can be seen in Fig. 8. Figure 9 shows the bifurcation diagrams of the generalized displacements associated with the four symmetric flexible modes incorporated in the unaugmented C1 configuration. Note that these displacements are normalized with respect to the "datum point" on the aircraft (see Fig. 1). In addition, $\dot{\eta}_i = 0$, $i = 1, 2, 3, 4$, for equilibria, and thus these states are not shown in Fig. 9.

Referring to Eqs. (1–6), the contribution of the elastic modes becomes apparent through the coupling that occurs via the aerodynamic forces and moments. Unlike the C0 configuration, the flexible models are characterized by relatively higher angles of attack as a result of this coupling.

In Fig. 10 both flexible configurations are shown relative to the rigid system as an $\alpha - \delta_{SHT}$ bifurcation diagram. Recall from Table 1 that in going from C0 to C1 and then C2 the frequency separation becomes smaller and the flexible modes, in particular the first symmetric mode, are much closer in frequency to the rigid-body modes; the overall dynamics of the system therefore become increasingly different from the rigid case in terms of the trim relationship and stability. It should be noted that all trim branches intersect at the point where structural deflections are zero in each mode (label A in Fig. 10), where the aerodynamic loading balances the structural forces. In addition, for configuration C2, the aircraft is unstable above $\alpha = 4.5^\circ$ and BPs 2 and 3 do not occur in this case. Instead, the aircraft response is characterized by larger elastic deflections and increased pitch response compared with the rigid and baseline-flexible models. Since the structural model is linear, as δ_{SHT} increases trailing edge down from point A in Fig. 10, it is reasonable to assume that the deflections are less representative. However, as in [22], we apply the model here over the full-α range.

Finally, modal analysis of these flexible configurations has revealed a significant effect on the stability characteristics of this aircraft. In particular, configuration C2 displayed a notable increase in the period of vibration of the short period mode. Figure 11 shows Bode plot frequency responses of all three versions of the model, linearized at $\alpha = 1.15^\circ$, for the pitch rate to δ_{SHT} transfer function. Differences in magnitude of vibration of the short period mode are noted; in particular, as the frequency of vibration of the flexible modes is reduced, it can be clearly seen that this has a direct effect on the frequency and damping characteristics of the short period mode.

V. Augmented Aircraft Analysis

A full-SCAS design accounting for structural modes would incorporate various elements (including notch filters) to achieve the appropriate filtering and sensing of the structural modes and thereby address the aerostructural coupling problem. However, in this paper, we consider simple idealized controllers in order to remove the pitch instabilities present in the model. The main objective is to evaluate the potential for the bifurcation analysis approach to explain

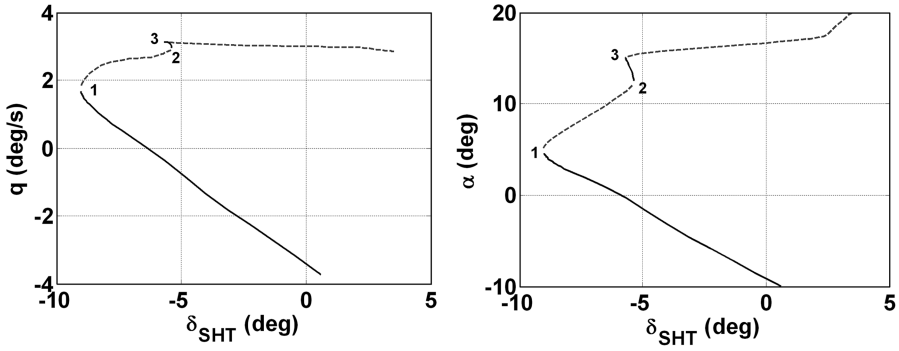

a) Pitch rate **b) Angle of attack**

Fig. 8 Bifurcation diagrams of rigid-body states of the unaugmented C1 configuration. BPs 1–3 correspond to those in Fig. 6.

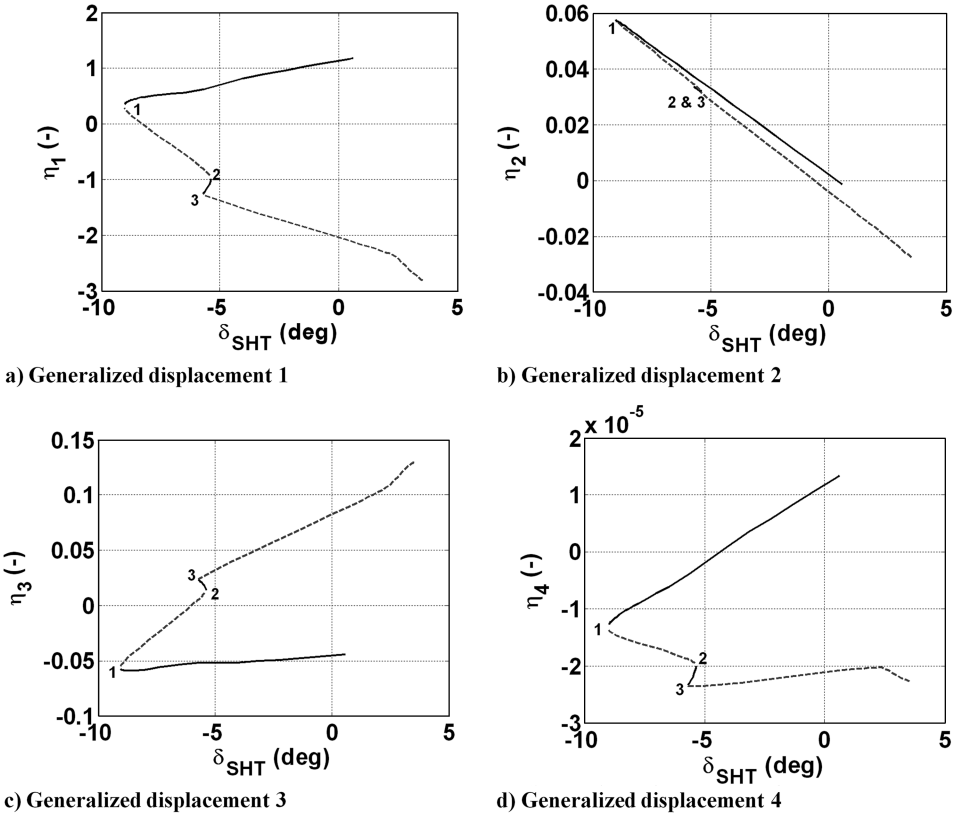

Fig. 9 Bifurcation diagrams of selected elastic states of the unaugmented C1 configuration. BPs 1–3 correspond to those in Fig. 6.

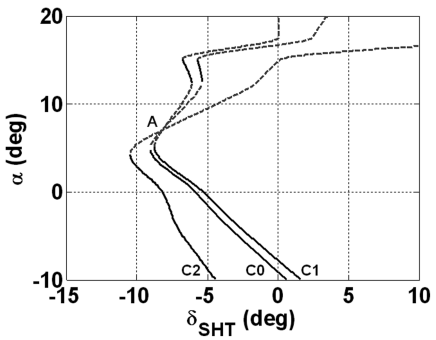

Fig. 10 Comparison of unaugmented aircraft flexible and rigid-body equilibria.

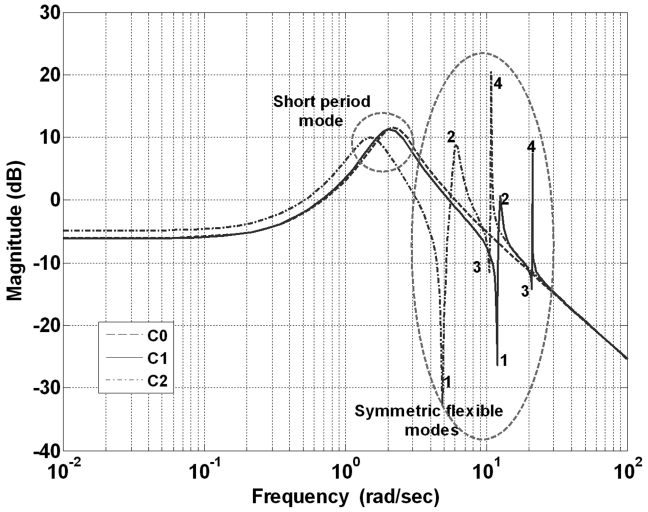

Fig. 11 Frequency response comparison of unaugmented configurations C0, C1, and C2 for the pitch rate response to δ_{SHT} input.

nonlinear phenomena due to the coupled aeroelastic system. To do so, we design an idealized controller for the C0 system, which effectively linearizes the system and provides desired dynamics, and apply it to the C1 and C2 versions of the model, where nonlinearities reappear due to the increased coupling. Similarly, a controller designed for C1 is implemented on C2.

Modern control techniques such as EA are suitable for multi-input–multi-output systems since they allow not only the system's poles to be placed at the desired locations, but also take advantage of the extra freedom arising from multiple inputs to shape the eigenvectors within the eigenspace. The EA technique used in this work is a state feedback approach based on populating a gain matrix, K, such that the resulting closed-loop system eigenvalues are moved to a set of desirable values. The EA process is incorporated within the continuation algorithm (using the AUTO software [6]), and the feedback command input parameter is defined as the CP, e.g., commanded α_{com}; the gain matrices are calculated quasi continuously at trim points of the aircraft model throughout the CP range. The resulting controller is a quasi-continuous form of standard gain scheduling, and the integration of the gain design within the continuation method is an important feature of the nonlinear tools described in this paper.

A. Control Law Synthesis Using Rigid-Body-State Feedback (SCAS-C0)

The EA technique was used to implement an idealized control law for the rigid-body model, C0, in order to stabilize the short period mode using δ_{SHT} as the only control effector. A transfer function $s/(s+20)$ was used to capture dynamics of the actuator, and a rigid-body state proportional/integral feedback of α was employed in the forward path of the SCAS, so that pilot input is now α_{com} (see Fig. 12). The actuator mode was unconstrained in the EA method (i.e., the eigenvalue associated with the actuator mode was not specified when calculating the required gains), whereas, the short period mode was placed (according to level 1 handling qualities of the Cooper–Harper Scale) at $-1.50 \pm 1.50i$. Rigid-body state feedback is adopted for this idealized controller. The calculated gains

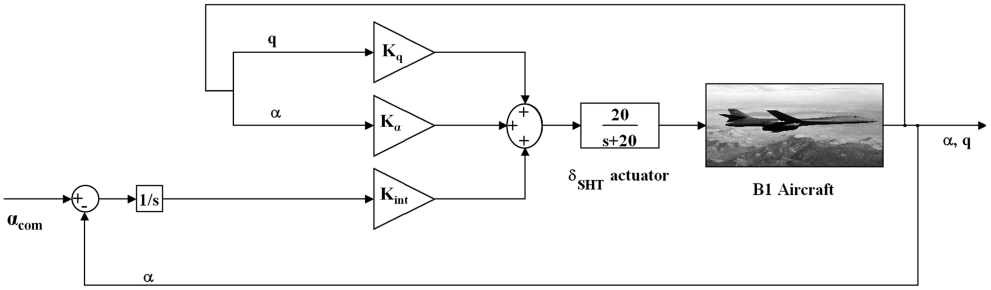

Fig. 12 Block diagram of the SCAS-C0.

were then stored in look-up tables to form a gain-scheduled controller that can then be implemented on each of the three vehicle configurations to assess the impact of the dynamic coupling when varying the frequencies of the flexible modes.

B. Control Law Using Full-State Feedback (SCAS-C1)

Another simple idealized controller was developed incorporating the control vanes (δ_{cv}) as an additional control effector, along with δ_{SHT} to define idealized control laws in an attempt to alleviate the effects induced by the flexible modes. A transfer function $50/(s + 50)$ [25] was used to represent the dynamics of the control vanes actuator. Full-state feedback is assumed, including the generalized displacements (i.e., the feedback variables are q, α, and η_i, $i = -1, 2, 3, 4$). In practice, this approach would require the use of state estimators, such as via Kalman filters (e.g., a similar approach was presented in [26]). The eigenvalues of the short period mode were again placed according to the Cooper–Harper Level 1 handling qualities, while the actuator modes were unconstrained. The eigenvalues of the flexible modes were placed at locations occupied by the C1 configuration, without SCAS, at a typical cruise flight condition. At these locations, the short period mode displays good frequency and damping characteristics, and the aircraft has good handling qualities indicating minimal impact from the elastic modes on the dynamics of the aircraft. The eigenvectors associated with both the Short Period and elastic modes were specified such that the elastic mode contributions to the pitch rate are eliminated or at least minimized. Table 4 lists all the described eigenvalue locations along with the desired frequencies and damping characteristics used when calculating the various gains with the EA method.

C. Analysis of System Augmented SCAS-C0 Controller

Unaugmented aircraft analysis results showed that without a SCAS the aircraft is unstable for $\alpha \geq 5.0°$. Therefore, stability augmentation is required, and in this section, the combined aircraft-SCAS system, designed as described in Sec. V.A using the rigid-body state feedback only (SCAS-C0) is examined.

1. Rigid-Body Model

The augmented C0 model has four states: α, q, δ_{SHT} and the controller integrator state. Bifurcation diagrams of the closed-loop reduced-order model are shown in Fig. 13. The addition of the SCAS-C0 has removed all instabilities seen in the unaugmented aircraft response, and the aircraft is now stable over the target α range of -10 to $20°$. The desired eigenvalues were achieved throughout this envelope.

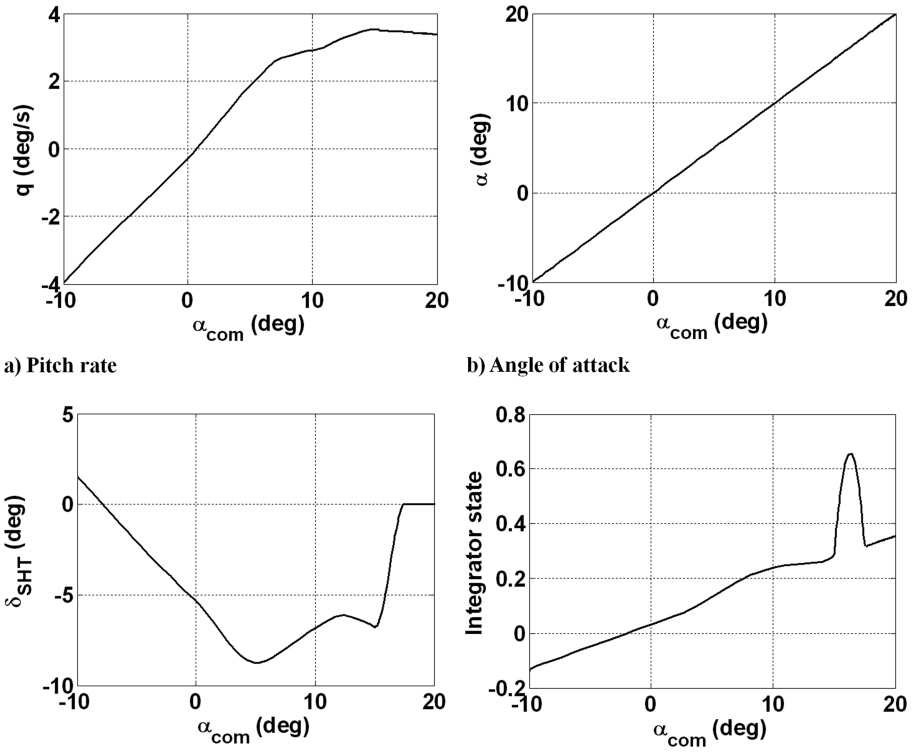

a) Pitch rate

b) Angle of attack

c) Symmetric horizontal tailplane

d) Integrator state

Fig. 13 Bifurcation diagrams of the C0+SCAS-C0 model.

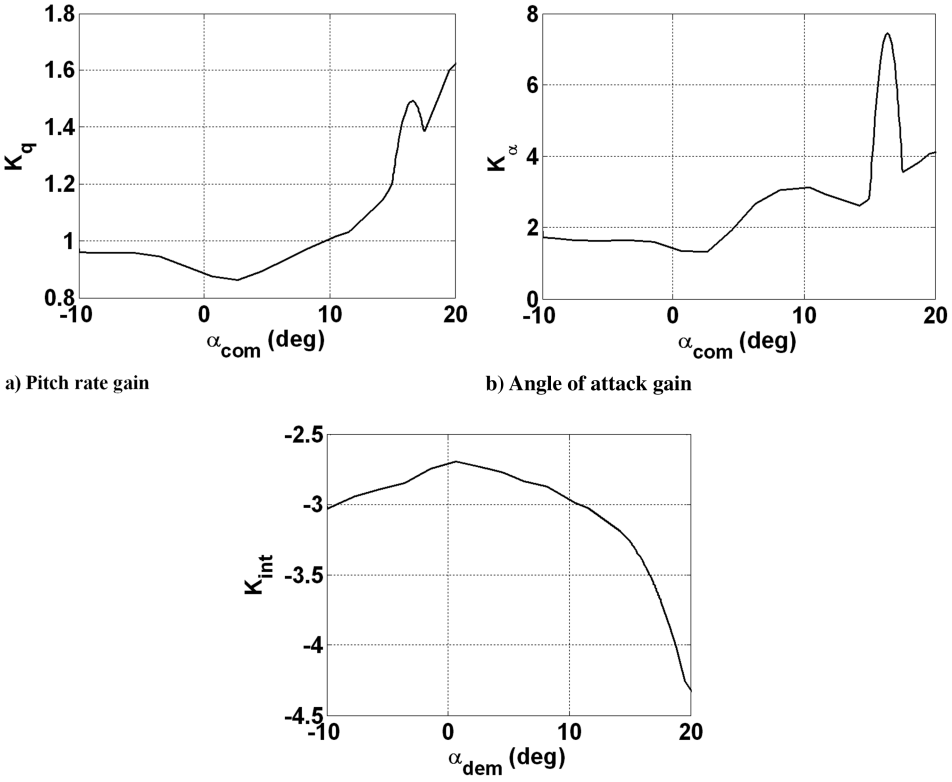

a) Pitch rate gain

b) Angle of attack gain

c) Integrator state gain

Fig. 14 Bifurcation diagrams of the C0+SCAS-C0.

The gains calculated using the EA method are plotted in Fig. 14. In general, higher gains are required to place the eigenvalues at the desired positions, in regions where bifurcations occur in the unaugmented system.

2. Flexible Models

To further investigate the effects induced by the flexible modes on the overall dynamics of the Rockwell B1 aircraft models, the SCAS-C0 is used with the two flexible versions of the aircraft (C1 and C2) defined in Table 2. The four elastic modes were added to the second-order rigid-body model along with the two modes introduced by the actuator and controller integrator. There are thus 12 states: α, q, δ_{SHT}, integrator, η_i, $\dot{\eta}_i$, $i = 1, 2, 3, 4$.

Bifurcation diagrams revealed that when the frequency separation between the rigid and flexible modes is adequate (configuration C1), the SCAS-C0 stabilizes the aircraft over the entire α range, i.e., -10 to 20°, with the bifurcation diagram for rigid-body and controller states similar to the results presented in Fig. 13. Modal analysis (not shown) reveals that although the aircraft is stable, the eigenvalues have slightly different values from those specified when calculating the gains. The incorporation of the flexible modes into the nonlinear model resulted in a dynamic change, although not to the extent that one of the aircraft modes becomes unstable, characterized by an interaction between the aircraft rigid and flexible modes as well as the controller modes. Therefore, the overall handling qualities of the aircraft are degraded, as the short period mode exhibits an increase in frequency and a decrease in damping as α_{com} is increased.

On the other hand, when the frequency margin between the rigid-body and the flexible modes is significantly reduced, i.e., configuration C2, the effects of the flexible modes become more dominant, such that the SCAS-C0 can no longer stabilize the aircraft fully, and a number of bifurcations occur at higher α. In particular, the short period mode becomes unstable resulting in a Hopf bifurcation and associated LCOs, as seen in Fig. 15.

Note that the solutions shown for periodic orbits are the maximum amplitude, and these were generated even for high α outside the validity range of the aerodynamic data. This was done in order to check for the possibility that the limit cycle solution branch arising at the Hopf bifurcation at $\alpha \approx 15°$ reenters the allowable envelope, which it does at $\alpha_{\mathrm{com}} \approx 15.3°$. It is, in fact, generally accepted that generating bifurcation diagrams beyond physical limits often allows additional steady-state branches to be found inside the limits. Table 5

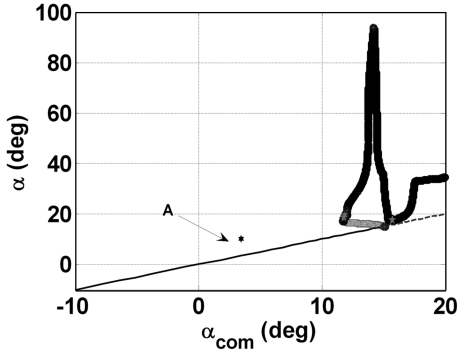

Fig. 15 Angle of attack bifurcation diagram for the C2 + SCAS-C0 model.

Table 5 BPs of the C2+SCAS-C0 model

La	CP α_{com}, deg	α, deg	Type
1	15.05	15.05	Hopf
2	15.08	15.20	Periodic fold
3	11.71	17.21	Periodic fold
4	11.76	17.76	Period doubling
5	11.98	19.30	Period doubling
6	12.02	19.93	Periodic fold
7	12.01	21.22	Periodic fold
8	11.87	19.62	Period doubling
9	11.80	18.52	Period doubling
10	15.40	17.35	Period doubling
11	15.72	17.36	Period doubling

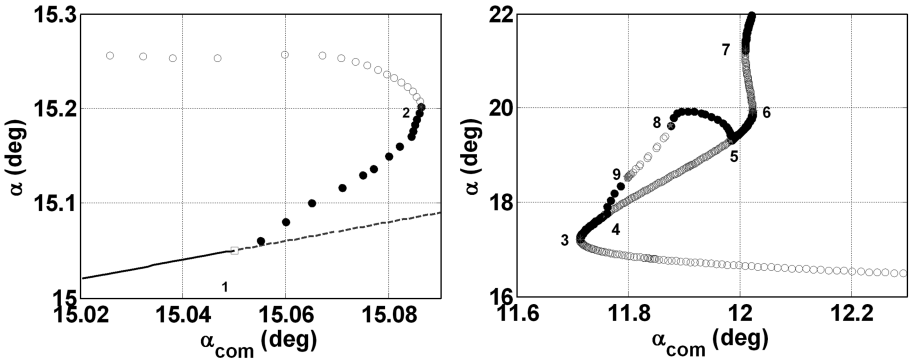

a) Magnified view of (a) showing BPs 1 and 2 b) Magnified view of (a) showing BPs 3-9

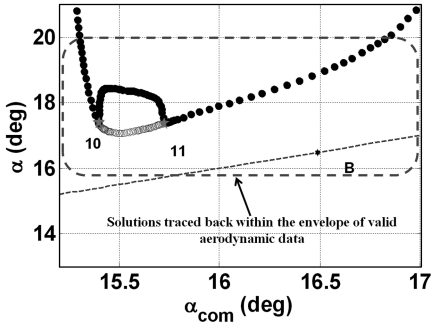

c) Magnified view of (a) showing BPs 10 and 11

Fig. 16 Magnified views of Fig. 15 showing all BPs.

lists all BPs identified within the allowable envelope, and they are also clearly shown in magnified views of Fig. 15 provided in Fig. 16.

As the CP reaches 15.05°, the system becomes unstable when the short period mode migrates across the imaginary axis denoted by label 1 in Fig. 16a. This is a supercritical Hopf leading to a stable LCO that grows in amplitude as α_{com} is increased until stability changes at the periodic fold bifurcation (label 2). A classical linear analysis would detect the eigenvalues crossing into the right-half plane at a point corresponding to label 1 in Table 5, and hence the equilibria instability, thus a LCO could be predicted. A nonlinear analysis, on the other hand, shows when a Hopf is subcritical or supercritical; if the former, there is a region (before reaching the Hopf point) where if a large enough disturbance occurs, the trajectory will end up on the LCO even though the linear analysis indicates stability. The nonlinear analysis reveals the possibility for the response to be unstable (with respect to the equilibria), and to be attracted to the stable LCO. It shows the structure governing the changes in stability and gives insight into the types of response that may arise.

This is an important feature of the nonlinear approach that can be beneficial for exhibiting the parameter dependence of the system dynamics, for example sensitivity studies relating to model uncertainty, or to atmospheric disturbances. The unstable LCOs arising from the periodic fold at label 2 become stable, as α increases, through a fold bifurcation (label 3) and as the α_{com} parameter is varied further stability is lost when the system exhibits a period doubling bifurcation (label 4). However, it is regained once again through another period doubling bifurcation (label 5) at $\alpha_{\text{com}} = 11.98°$. Note that secondary branches of periodic solutions emanate from these two BPs, characterized by a period twice that of the LCOs on the primary branch. Also, secondary period doubling bifurcations (labels 8 and 9) occur on this branch, and it is expected that further period doubling bifurcations may occur, but no attempt has been made to further generate these. Various other BPs were obtained when generating solutions further along this branch; these were not thoroughly examined, however, are indicated in Figs. 16b and 16c. Time history simulations were run, using the same model, at selected points of interest in the bifurcation diagrams. Figures 17 and 18 show responses of the aircraft corresponding to solutions from a nontrim point expected to yield a stable response (point A in Fig. 15) and a point on the unstable branch (point B in Fig. 16c). Note that in Fig. 18

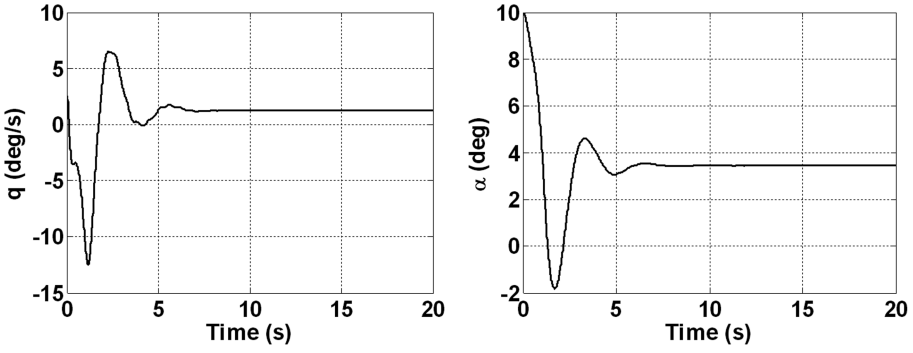

a) Pitch rate b) Angle of attack

Fig. 17 Time history simulation of the C2 + SCAS-C0 model at CP = $\alpha_{\text{com}} = 3.45°$ indicated as point A in Fig. 15. The response settles on the stable branch of equilibria.

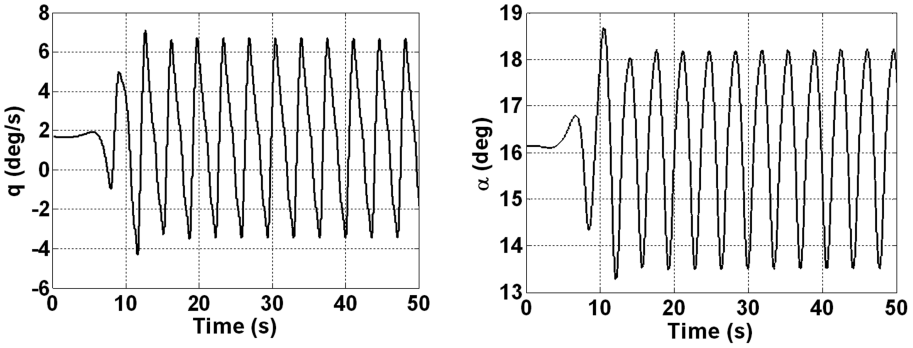

a) Pitch rate b) Angle of attack

Fig. 18 Time history simulation of the C2+SCAS-C0 model at CP $= \alpha_{com} = 16.5°$ indicated as point B in Fig. 16c. The response converges to a stable LCO.

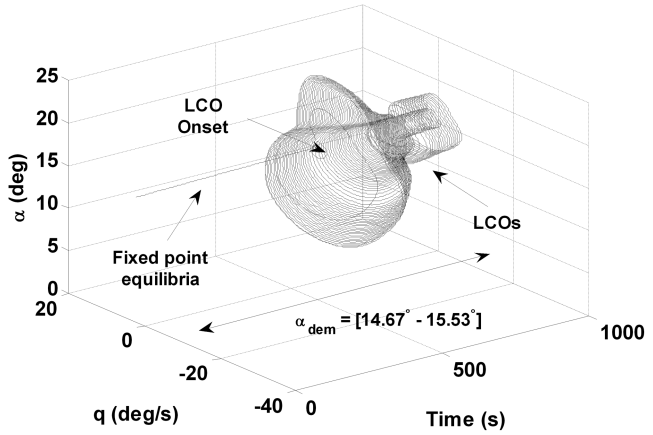

Fig. 19 Time history simulation of the flexible C2+SCAS-C0 model for α_{dem} varied from 14.8 to 15.5°.

the simulation shows that the solution is initially unstable, but quickly converges to a stable LCO at the same value of α_{com} as can be predicted from Fig. 16c.

Figure 19 shows a further time history simulation of the C2 +SCAS-C0 model, and was generated by increasing α_{com} the input (which corresponds to the CP in the bifurcation diagram) in a slow (quasi-steady) manner; a rate of 15×10^{-6} deg/s was used. The simulation clearly identifies the onset of large-amplitude LCOs at $\alpha \approx 15°$ although the dynamic structure of the system would not be evident from the time history trajectory alone. It can be observed that the initial manifestation of the bifurcation from stable equilibrium appears (correctly) to be supercritical. Also, it can be seen that a jump to large-amplitude LCO occurs, followed by period doubling. However, a deep understanding of what the structure is, the parameter dependence of the various stable and unstable solutions, and hence an ability to predict and modify the behavior is only available with the help of the bifurcation diagrams.

Time history simulations were also generated for other initial conditions and input variations, and comparisons with bifurcation

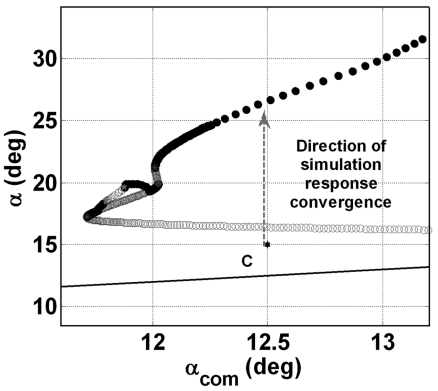

a) Magnified view of Fig. 15

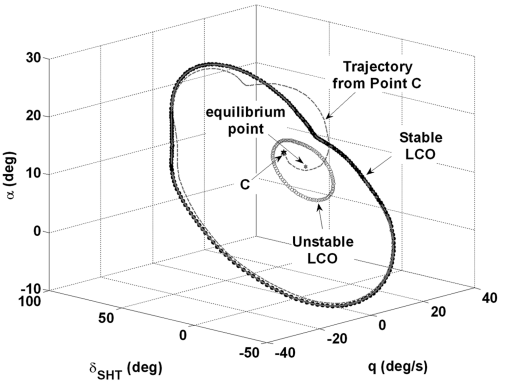

b) Sub-phase-space plot showing steady-states and trajectory from point C

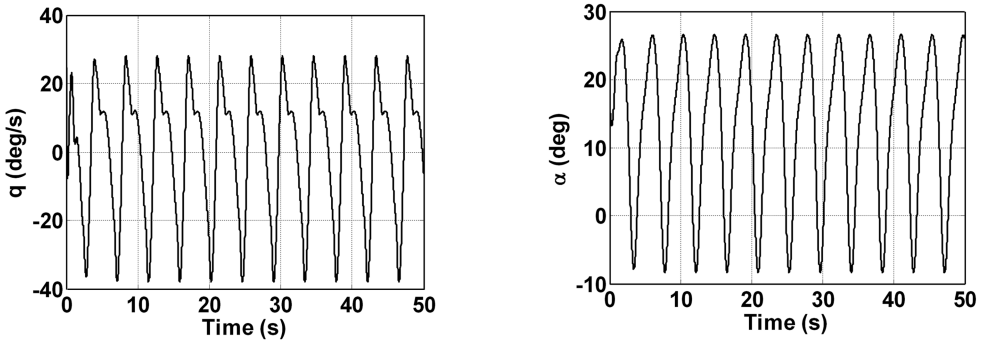

c) Time history simulation results

Fig. 20 Behavior of C2+SCAS-C0 model at $\alpha_{com} = 12.5°$. Time history initial condition is point C in Fig. 20a.

analysis were made to investigate the correlation. The results matched as expected, although unstable branches are obviously not clear from time histories. A further example of the benefits gained from using the bifurcation approach to supplement classical tools when nonlinearities are present is shown in Fig. 20. The time history results clearly indicate how the response quickly converges to a stable periodic orbit (not identified in linear analysis); the nonlinear simulation α response gives no indication of the presence of the unstable LCO near point C.

Note that, although point C appears to be closer to the stable equilibria than the stable LCO, it converges on the stable LCO and is not repelled by the unstable LCO towards the equilibria. This example reveals that the use of simulations alone to predict the behavior of the system is insufficient, as this classical method requires very specific starting solutions in order to detect the nonlinear behavior shown to occur using the bifurcation method. The bifurcation analysis shows where time histories should be run to provide additional information, for example transient responses. Thus, the approach used in this work has the potential to reveal the structure of the dynamic system and hence to minimize the need for large numbers of time history runs. It therefore reduces the computational burden in nonlinear analysis.

D. System Augmented Using SCAS-C1 Controller

The use of rigid-body state feedback (SCAS-C0) was shown to be less suitable in stabilizing the flexible vehicle when dynamic coupling occurs between the lowest elastic mode and the rigid-body modes, leading to aircraft instability and degraded handling qualities. In this section, the use of full-state feedback (SCAS-C1) in alleviating the dynamic coupling is investigated.

The augmented system analyzed in this section includes the two rigid-body states (α and q), four elastic modes (η_i, $\dot{\eta}_i$, $i = 1, 2, \ldots, 4$), along with the three modes introduced by the actuators and the controller (δ_{SHT}, δ_{cv}, and the integrator state), resulting in a flexible model with 13 states.

The gains calculated using the EA method are shown in Fig. 21. Again, they are in general of larger magnitude in regions where the nonlinear behavior exhibited by the aircraft is strongly present. In other words, in order to remove the instabilities shown to occur in the previous analysis, i.e., using the SCAS-C0, high gains are required. In addition, it is also noted that the δ_{cv} gains are generally slightly higher than the equivalent gains related to the δ_{SHT} control effector in these regions, which implies that the control power required to decouple the elastic modes from the rigid-body modes is high. We also note that gains for some of the generalized displacement feedback paths are nonlinear with respect to α despite the fact that the structural dynamics model is linear.

Figure 22 shows a comparison of the bifurcation results obtained for both flexible versions of the aircraft model (C1and C2) using SCAS-C1. The control law stabilizes both models, and hence removes the unstable behavior obtained previously when using rigid-body state feedback only. Modal analysis (not shown) reveals that the two models have different handling qualities with configuration C1

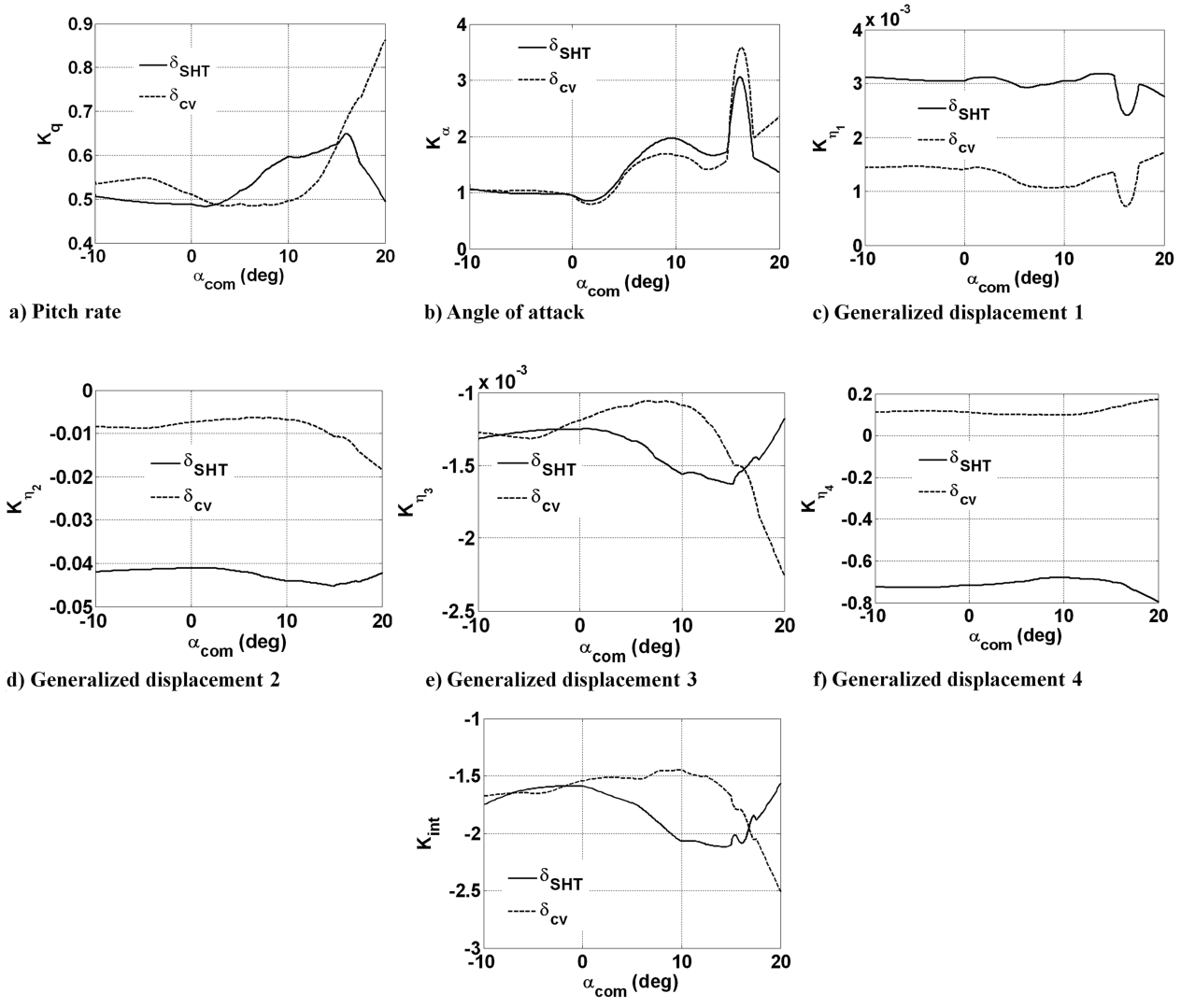

Fig. 21 Gains to stabilize the flexible models for use with the SCAS-C1.

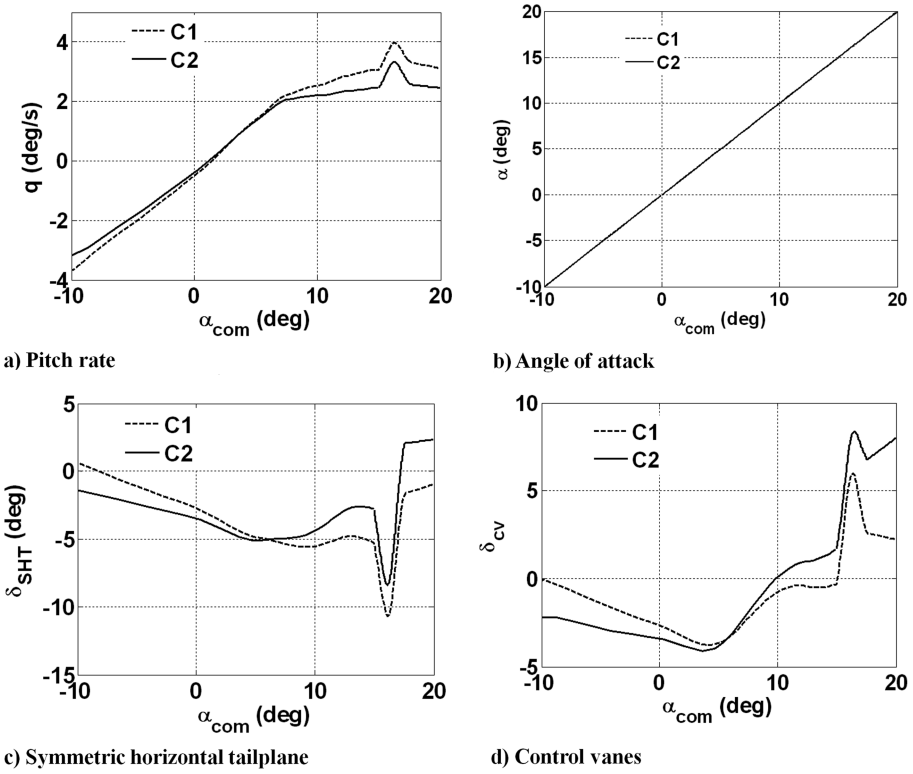

Fig. 22 Comparison of selected bifurcation diagrams for the C1 and C2 flexible models with the SCAS-C1. Note that, for both configurations, the results shown are stable equilibria for the entire α_{com} range.

satisfying the criteria defined in Table 4, whereas for configuration C2 both the short period mode and elastic mode 3 have lower damping coefficients due to the aerostructural coupling. In fact the short period roots move away from the level 1 handling qualities envelope when $\alpha \geq 15°$. Therefore, even though the effects of flexibility are minimized by stabilizing the aircraft over the entire α range, their impact on handling qualities remains notable, thus requiring an improved control law. This should be achieved using a SCAS designed for configuration C2 which produces the desired eigenstructure throughout the α_{com} range.

VI. Conclusions

The application of bifurcation and continuation methods has been shown to be a powerful tool in the analysis of flexible aircraft dynamics in the presence of nonlinearities in the model. Results for both rigid-body and elastic configurations of varying levels of structural flexibility demonstrated the efficiency of the methods to reveal changes in qualitative dynamics between the different cases. These significant bifurcation phenomena are present when the frequencies of the flexible modes are much closer to those of the rigid-body short period mode, despite the fact that the structural dynamics in the models are linear here.

The multiple steady-state solutions and associated LCOs arise, in the Rockwell B1 model considered here, when the stability augmentation system does not adequately account for the flexible mode dynamics. Time history analysis supported these findings. However, when used alone (i.e., without guidance from bifurcation analysis results), the simulation outputs provide no insight into the nature of any underlying instabilities, their parameter dependence, or nearly scenarios that could be very undesirable. This is because each simulated response is unique to its specific initial conditions and input variations, and a series of such runs can easily miss significant phenomena. Therefore, to uncover such information using a classical approach would in general require a very large number of simulations, even with the knowledge (from linear analysis) of where equilibria lose stability.

The continuation/bifurcation, however, is shown to provide the "global" insight to develop an understanding of the underlying dynamics in a multiple-attractor nonlinear system. In doing so it reveals where more detailed investigations (by time histories and/or other approaches) must be targeted. Thus, time history simulations remain important in order to evaluate transient effects near interesting phenomena, to determine the influence of trajectories starting away from the steady states and, sometimes, to check for additional steady states not yet identified in the numerical continuation.

The aircraft mathematical model used in this paper to illustrate the benefits of bifurcation analysis was implemented in a low-order form and made use of relatively simple idealized control laws. However, the approach is well suited to higher-order, more complex models (since bifurcations are usually associated with only one or two eigenvalues crossing the imaginary axis at any particular set of parameter values), provided the model is smooth. In fact, it may be argued that the higher the order and the degree of nonlinearity in the model, the greater the time savings obtained by using bifurcation analysis to complement classical tools.

References

[1] Wright, J. R., and Cooper, J. E., *Introduction to Aircraft Aeroelasticity and Loads*, Wiley, Hoboken, NJ, 2007, pp. 211, 257–262.

[2] Meriovitch, L., and Tuzcu, I., "Time Simulations of the Response of Manoeuvring Flexible Aircraft," *Journal of Guidance, Control, and Dynamics*, Vol. 27, No. 5, Sept.–Oct. 2004, pp. 814–828. doi:10.2514/1.2392

[3] Waszak, M. R., and Schmidt, D. K., "Flight Dynamics of Aeroelastic Vehicles," *Journal of Aircraft*, Vol. 25, No. 6, 1988, pp. 563–571. doi:10.2514/3.45623

[4] Schimdt, D. K., and Raney, D. L., "Modelling and Simulation of Flexible Flight Vehicles," AIAA Modelling and Simulation Technologies Conference and Exhibit, AIAA Paper 98-4359, Boston, MA, 1998.

[5] Etkin, B., and Reid, L. D., *Dynamics of Flight, Stability and Control*, Wiley, New York, 1996, pp. 120–125.

[6] Doedel, E., Champneys, A., Fairgrieve, T., Kuznetsov, Y., Sandstede, B., and Wang, X., "AUTO 97: Continuation and Bifurcation Software for Ordinary Differential Equations (with Homcont)," AUTO 97

Continuation Software User's Manual, Concordia Univ., Montreal, 1998.

[7] Dhooge, A., Govaerts, W., Kuznetsov, Y., Mestrom, W., Riet, A., and Sautois, B., "MATCONT and CL MATCONT: Continuation Toolboxes in MATLAB," MATCONT User's Manual, Gent Univ., Belgium, The Netherlands, 2003.

[8] Carroll, J. V., and Mehra, R. K., "Bifurcation Analysis of Nonlinear Aircraft Dynamics," *Journal of Guidance, Control, and Dynamics*, Vol. 5, No. 5, 1982, pp. 529–536. doi:10.2514/3.56198

[9] Lowenberg, M., "Bifurcation Analysis of Multiple-Attractor Flight Dynamics," *Philosophical Transactions of the Royal Society A: Mathematical, Physical and Engineering Sciences*, Vol. 356, No. 1745, 1998, pp. 2297–2319. doi:10.1098/rsta.1998.0275

[10] Zagaynov, G. I., and Goman, M. G., "Bifurcation Analysis of Critical Aircraft Flight Regimes," *Proceedings of the 14th Congress of ICAS*, 84-4.2.1, Toulouse, France, 1984.

[11] Jahnke, C. C., and Culick, F. E. C., "Application of Bifurcation Theory to the High-Angle-of-Attack Dynamics of the F-14," *Journal of Aircraft*, Vol. 31, No. 1, 1994, pp. 26–34. doi:10.2514/3.46451

[12] Lowenberg, M. H., "Bifurcation Analysis as a Tool for Post Departure Stability Enhancement," AIAA Atmospheric Flight Mechanics Conference, AIAA Paper 1997-3716, New Orleans, LA, 1997.

[13] Guicheteau, P., "Bifurcation Theory: a Tool for Nonlinear Flight Dynamics," *Philosophical Transactions of the Royal Society A: Mathematical, Physical and Engineering Sciences*, Vol. 356, No. 1745, 1998, pp. 2181–2201. doi:10.1098/rsta.1998.0269

[14] Avanzini, G., and de Matteis, G., "Bifurcation Analysis of a Highly Augmented Aircraft Model," *Journal of Guidance, Control, and Dynamics*, Vol. 20, No. 4, 1997, pp. 754–759. doi:10.2514/2.4108

[15] Goman, M. G., and Khramtsovsky, A. V., "Global Stability Analysis of Nonlinear Aircraft Dynamics," AIAA Guidance, Navigation, and Control Conference and Exhibit, AIAA Paper 97-3721, New Orleans, LA, 1997.

[16] Littleboy, D., and Smith, P., "Using Bifurcation Methods to Aid Nonlinear Dynamic Inversion Control Law Design," *Journal of Guidance, Control, and Dynamics*, Vol. 21, No. 4, 1998, pp. 632–638. doi:10.2514/2.4282

[17] Paranjape, A., Sinha, N. K., and Ananthkrishnan, N., "Use of Bifurcation and Continuation Methods for Aircraft Trim and Stability Analysis: A State-of-the-Art," *Journal of Aerospace Sciences and Technologies*, Vol. 60, No. 2, 2008, p. 85.

[18] Roberts, I., "Analysis of Non-Linear Aeroelastic Systems Using Numerical Continuation," Ph.D. Thesis, Univ. of Bristol, Bristol, England, U.K., 2004.

[19] Kim, K., "Nonlinear Aeroelastic Analysis of Aircraft Wing-with-Store Configurations," Ph.D. Thesis, Texas A&M Univ., College Station, TX, 2004.

[20] Nichkawde, C., "Nonlinear Aeroelastic Analysis of High Aspect-Ratio Wings Using the Method of Numerical Continuation, Master's Thesis, Texas A&M Univ., College Station, TX, 2006.

[21] Siepenkötter, N., and Alles, W., "Stability Analysis of the Nonlinear Dynamics of Flexible Aircraft," *Journal of Aerospace Science and Technology*, Vol. 9, No. 2, 2005, pp. 135–141. doi:10.1016/j.ast.2004.10.005

[22] Waszack, M. R., Davidson, J. B., and Schmidt, D. K., "A Simulation Study of the Flight Dynamics of Elastic Aircraft: Volume 1: Experiment, Results and Analysis," NASA TR 4102, 1987.

[23] Waszack, M. R., Davidson, J. B., and Schmidt, D. K., "A Simulation Study of the Flight Dynamics of Elastic Aircraft: Volume 2: Data," NASA TR 4102, 1987.

[24] Strogatz, S., *Nonlinear Dynamics and Chaos*, Addison Wesley Longman, Reading, MA, 1994.

[25] Wykes, J., Byar, T., MacMiller, G., and Greek, D., "Analyses and Tests of the B-1 Aircraft Structural Mode Control System," NASA TR 144887, 1980.

[26] Wykes, J., Mori, A., and Hoge, H., "Combined Vertical and Lateral Identical Location of Accelerometer and Force System," U.S. Patent No. 3902686, filed 17 Oct. 1973.